

ARTICLE OPEN



Resolution dependence of CO₂-induced Tropical Atlantic sector climate changes

W. Park¹ and M. Latif^{1,2}

A long-standing problem in state-of-the-art climate models is the Tropical Atlantic (TA) warm sea surface temperature (SST) bias, which goes along with major biases in large-scale atmospheric circulation. Here we show that TA-sector climate changes forced by increasing atmospheric carbon dioxide (CO₂) levels are sensitive to model resolution. Two versions of a climate model employing greatly varying atmospheric resolution and exhibiting very different warm bias strength are compared. The version with high atmospheric resolution features a small SST bias and simulates an eastward amplified SST warming over the equatorial Atlantic, in line with the observed SST trends since the mid-20th century. On the contrary, the version with coarse atmospheric resolution exhibits a large SST bias and projects relatively uniform SST changes across the equatorial Atlantic. In both model versions, the warming pattern resembles the pattern of interannual SST variability simulated under present-day conditions. Atmospheric changes also vastly differ among the two climate model versions. In the version with small SST bias, a deep atmospheric response is simulated with a major change in the Walker circulation and strongly enhanced rainfall over the equatorial region, whereas the atmospheric response is much weaker and of rather different character in the model with large SST bias. This study suggests that higher atmospheric resolution in climate models may enhance global warming projections over the TA sector.

npj Climate and Atmospheric Science (2020)3:36; <https://doi.org/10.1038/s41612-020-00139-6>

INTRODUCTION

The atmospheric carbon dioxide (CO₂) concentration has risen by more than 40% above preindustrial levels in response to anthropogenic emissions, which largely contributed to the observed global surface warming since the mid-20th century¹. Atmospheric CO₂-levels will continue to rise during the next decades under any plausible scenario², which will promote additional warming. The salient features of the temperature change distribution in response to increasing atmospheric CO₂ concentrations were successfully projected with a climate model 30 years ago³. However, climate models exhibit still large biases such as those in sea surface temperature (SST)⁴, limiting their ability to project climate change in response to anthropogenic forcing.

Uncertainty in climate change projections for the 21st century is especially large on the regional scale where besides internal variability⁵ climate model bias is a major contributor^{6–10}. In many climate models, biases are particularly large over the Tropical Atlantic (TA), with a prominent warm SST bias over the eastern TA^{11–17}. A major problem in these models is their inability to capture the seasonal cold-tongue evolution in the eastern and central TA, a cooling of SST in boreal spring and summer. The biases in SST are associated with biases in large-scale atmospheric circulation, which are reflected, for example, in erroneous wind and rainfall patterns^{18,19}. The errors in the mean state also bias the interannual variability over the TA²⁰ and Atlantic tropical storm activity²¹.

It is thus of great interest whether the climate response to increasing atmospheric CO₂-levels is sensitive to the mean state and in particular to the strength of the warm SST bias over the eastern TA (hereafter warm bias). To address this question, we performed simulations with a climate model forced by increasing atmospheric CO₂ concentrations. Two versions of the model have been used, which only differ in atmospheric resolution and show

quite different performance in simulating SST over the TA under present-day conditions. In particular, the two model versions exhibit very different warm bias strength. To our knowledge, so far no study has been performed that attempts to explicitly investigate the influence of atmospheric resolution in climate change projections over the TA sector. We note that differing atmospheric resolution impacts the overall dynamics of the climate model.

RESULTS

SST trends in observations, low- and high-resolution model

We use two configurations of the Kiel Climate Model (KCM)²²: one employs the atmosphere general circulation model (AGCM) ECHAM5 with a spectral horizontal resolution of T42 (~2.8°) and 31 vertical levels (low-resolution, hereafter KCM-LR), and the other T255 (~0.47°) and 62 levels (high-resolution, hereafter KCM-HR). Relative to KCM-LR, not only the warm bias strength is strongly reduced but also the representation of the SST seasonal cycle and interannual SST variability in the TA much enhanced in KCM-HR^{23,24}. Increasing the atmospheric resolution improves the large-scale atmospheric circulation, in particular surface winds, in stand-alone mode with specified observed SST and in coupled mode²⁴. Sahel rainfall and predictability of its onset due to improved Atlantic cold-tongue development are enhanced too at sufficiently high atmosphere model resolution²⁵. Most of the improvements are due to more realistic meridional and vertical zonal momentum transports in the atmosphere and better representation of orography surrounding the TA²⁶.

KCM-LR exhibits a large warm bias in a “present-day” control integration (“Methods”) of the model (Fig. 1d) with respect to observed SST during 1971–2000 (Fig. 1a), which is similar to the ensemble-mean warm bias⁴ calculated from models participating in the Coupled Model Intercomparison Project phase 5²⁷. KCM-HR

¹GEOMAR Helmholtz Centre for Ocean Research Kiel, Kiel, Germany. ²Kiel University, Kiel, Germany. ✉email: wpark@geomar.de

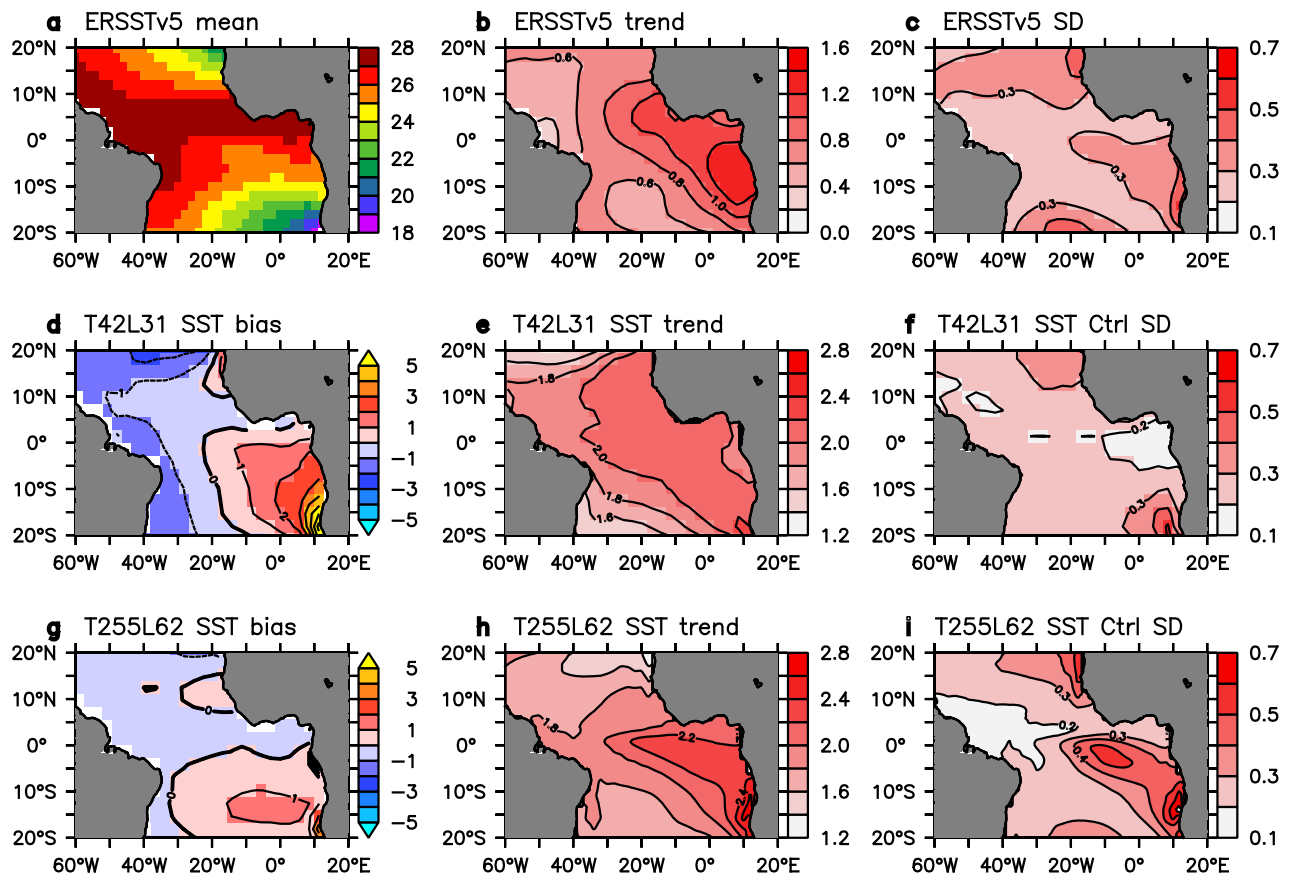


Fig. 1 Mean state, trend, and variability of SST. **a** Observed climatological mean SST (°C, 1971–2000) from ERSSTv5³³. **b** Linear SST trends during 1951–2018 from ERSSTv5 (CI = 0.2 °C) and **c** standard deviation of the detrended data (CI = 0.1 °C). Annual-mean SST bias (°C) in the climate model (KCM) version with **d** a coarse-resolution atmospheric component (KCM-LR) and **g** high-resolution atmospheric component (KCM-HR). Observations and KCM-HR data are interpolated onto the T42 grid, and the area mean is removed (CI = 1 °C). Linear ensemble-mean SST trends, calculated over all 70 years from KCM-LR (**e**) and from KCM-HR (**h**) (CI = 0.2 °C). Standard deviations of SST from control simulations with KCM-LR (**f**) and KCM-HR (**i**) (CI = 0.1 °C). Annual-mean data are used.

exhibits a much-reduced warm bias (Fig. 1g) in comparison to KCM-LR. We performed ensemble global warming simulations with the two models, in which the atmospheric CO₂ concentration increases at a rate of 1% per year until it doubles after 70 years. Each ensemble consists of five members starting from different oceanic and atmospheric conditions taken at 10-year intervals from the respective control integration. The transient climate sensitivity of the two KCM versions is virtually identical, as shown by the time evolution of the ensemble-mean globally averaged surface air temperature (GSAT) (Supplementary Fig. 1). The response to the increasing atmospheric CO₂-levels is shown in terms of the ensemble-mean linear trends calculated over the full 70 years of the global warming simulations. SST trends over all tropical oceans projected by KCM-LR and KCM-HR are shown in Supplementary Fig. 2b, c, respectively, together with the observed trends during 1951–2018 (Supplementary Fig. 2a). Annual-mean data are used throughout the paper.

A basin-wide increase of the SST over the TA has been observed since the mid-20th century with largest warming trends over the eastern TA slightly south of the equator (Fig. 1b), where interannual variability of SST also is large (Fig. 1c). It is unclear whether the observed trends over the eastern TA are externally forced or a realization of internal multidecadal variability. KCM-LR only exhibits little zonal variation in the projected SST-trend pattern in the region 10°N–10°S (Fig. 1e). In particular, large SST warming in KCM-LR is simulated in the southeastern TA close to the African coast where interannual SST variability attains its maximum in the control integration (Fig. 1f). The SST response in

KCM-HR is more equatorially confined and exhibits a pronounced zonal variation across the equatorial region with largest warming in the east (Fig. 1h), which is consistent with the observed SST trends. As in observations and KCM-LR, the largest warming trends in KCM-HR are projected where interannual SST variability is largest (Fig. 1i). The warming trends in the models are considerably larger than in observations, which is likely due to the stronger CO₂-forcing in the global warming simulations.

Oceanic and atmospheric trends

The net surface heat flux response in KCM-LR is relatively noisy and there is virtually no large-scale heating of the atmosphere by the ocean (negative heat fluxes, Fig. 2a), except for the northernmost (southernmost) warming lobes in the northern (southern) TA. In KCM-HR, large-scale heating of the atmosphere is obvious over the eastern and central equatorial Atlantic and over the southeastern TA close to the African coast (Fig. 2b), which are the regions of largest SST warming (Fig. 1h). The opposite behavior is found over the northern TA in which maximum SST warming is caused by air-sea fluxes. Changes in dynamic sea level (DSL), the departure from the globally averaged sea level, also differ. In particular, the DSL rise in the eastern equatorial TA is considerably larger in KCM-HR (Fig. 2d) in comparison to that in KCM-LR (Fig. 2c), which indicates more strongly reduced easterly zonal wind stress across the equator in KCM-HR (Fig. 2d).

The two KCM versions simulate very different CO₂-induced atmospheric changes. KCM-LR simulates a weaker and qualitatively

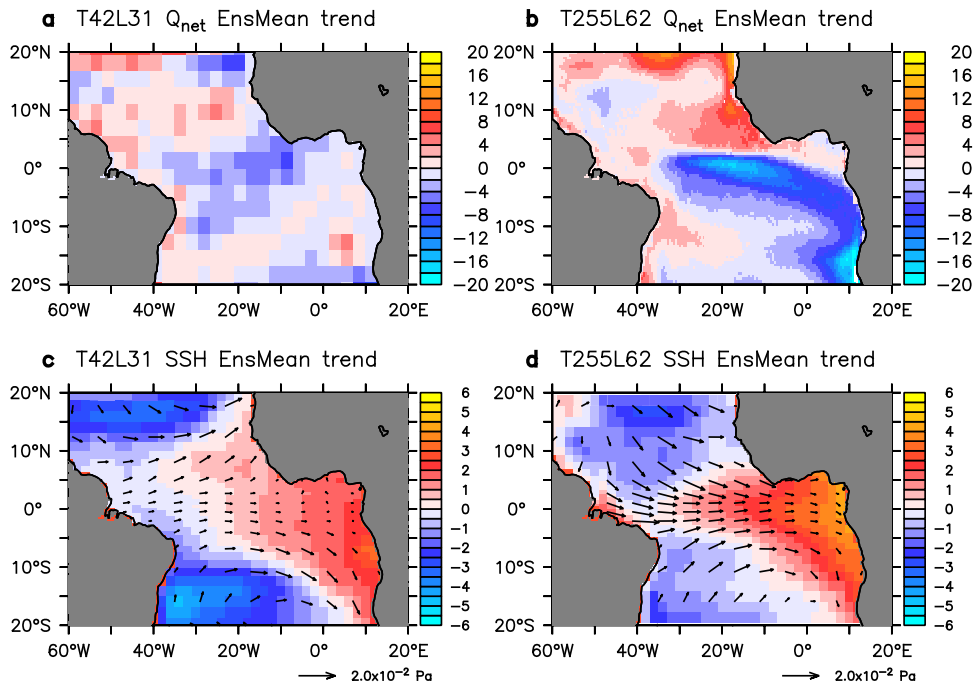


Fig. 2 Surface heat flux, dynamic sea level, and wind stress changes. Ensemble-mean trends, calculated over all 70 years, of **a, b** net surface heat flux (Q_{net} ; W m^{-2} per 70 years), and **c, d** dynamic sea level (DSL; cm per 70 years) and wind stress (Pa per 70 years) calculated from KCM-LR (**a, c**) and from KCM-HR (**b, d**). Wind stress vectors are plotted every 3rd grid point on the ocean model grid.

different atmospheric response in comparison to KCM-HR. With respect to rainfall, KCM-LR yields an overall weak response (Fig. 3a), while KCM-HR simulates a much stronger response over large regions of the TA (Fig. 3b). Major differences between the two coupled models are observed north of the equator where KCM-LR hardly projects any rainfall changes while KCM-HR simulates strongly reduced rainfall. Moreover, rainfall along the equator intensifies much more and extends farther to west in KCM-HR in comparison to KCM-LR. Thus, KCM-HR projects enhanced rainfall over the entire equatorial Atlantic. The sea level pressure (SLP) trends in KCM-LR are of the same sign over almost the entire TA sector with the exception of the southwestern TA (Fig. 3c). In KCM-HR, the SLP trends are characterized by an east–west dipole with enhanced SLP over the western and reduced SLP over the eastern TA (Fig. 3d). Largest differences in the SLP response between the two models are observed over the northwestern TA where a decrease in SLP is simulated in KCM-LR as opposed to an increase in KCM-HR.

The middle-troposphere vertical velocity response at the 500-hPa level is relatively weak in KCM-LR (Fig. 3e), while KCM-HR simulates strong upward motion over the eastern equatorial Atlantic and strong downward motion to the west off the equator (Fig. 3f). Further, there is more consistency between the mid-troposphere vertical velocity and rainfall in KCM-HR. For example, the largest upward motion in KCM-LR is simulated in the southeastern TA, but upward motion only leads to a rainfall anomaly south of 10°S . In contrast, the large vertical velocity signal over the eastern equatorial Atlantic in KCM-HR is associated with a strong rainfall anomaly. The upper-troposphere velocity potential at the 200-hPa level, describing large-scale horizontal wind divergence or convergence and thus regions of upward or downward motion below the level, respectively, is shown in Fig. 3g, h. KCM-LR exhibits a rather uniform negative trend pattern, indicating wide divergence (Fig. 3g). In contrast, KCM-HR's upper-troposphere velocity potential features a dipolar pattern, associated with divergence over the eastern TA and equatorial Africa and convergence over the western TA and South America (Fig. 3h).

The response of the equatorial zonal mass overturning streamfunction is relatively uniform in KCM-LR (Fig. 4a) and does not suggest a major reorganization of the Walker circulation. There is an anticlockwise circulation change west of Greenwich meridian and a clockwise change to the east in KCM-HR, implying anomalous upward motion near 0°E (Fig. 4b), consistent with vertical velocity (Fig. 3f) and rainfall (Fig. 3b). The CO_2 -induced atmospheric changes over the equatorial Atlantic in KCM-HR support the picture of a deep atmospheric response and a major change in the Walker circulation that is reminiscent of variability associated with the Atlantic Niño also termed zonal mode²⁸, a behavior that is not observed in KCM-LR.

Role of SST-trend pattern, mean state, and model resolution

In order to obtain further insight into the factors that determine the KCM's response to increasing atmospheric CO_2 -levels, we performed uncoupled experiments with the atmospheric component of the KCM, ECHAM5 ("Methods", Table 1). The major focus here is on the equatorial region which is supposed to have a strong influence on the atmospheric variability. Results only are shown for rainfall (Figs. 5, 6, and Supplementary Fig. 3). We note that the continental response is mostly due to model climatology, and land surface temperature is calculated interactively from the surface energy balance.

First, we address the role of remote forcing in the TA-sector climate response²⁹. Three experiments with the high-resolution AGCM (T255L62, ECHAM5-HR) are conducted, in which the SST trends from the coupled-model ensemble with KCM-HR (Fig. 1h and Supplementary Fig. 2c) are specified over different regions and added to the observed monthly SST climatology. First, the SST trends only are specified over the TA (labeled TA); second, only over the tropical Indo-Pacific (TIP) (labeled TIP) and third, globally outside of the TA (labeled nTA). The rainfall response (Fig. 5a–c) is calculated relative to a control run with observed SST climatology specified.

When only the SST trends over the TA drive the model, the increase in rainfall over the equatorial Atlantic observed in

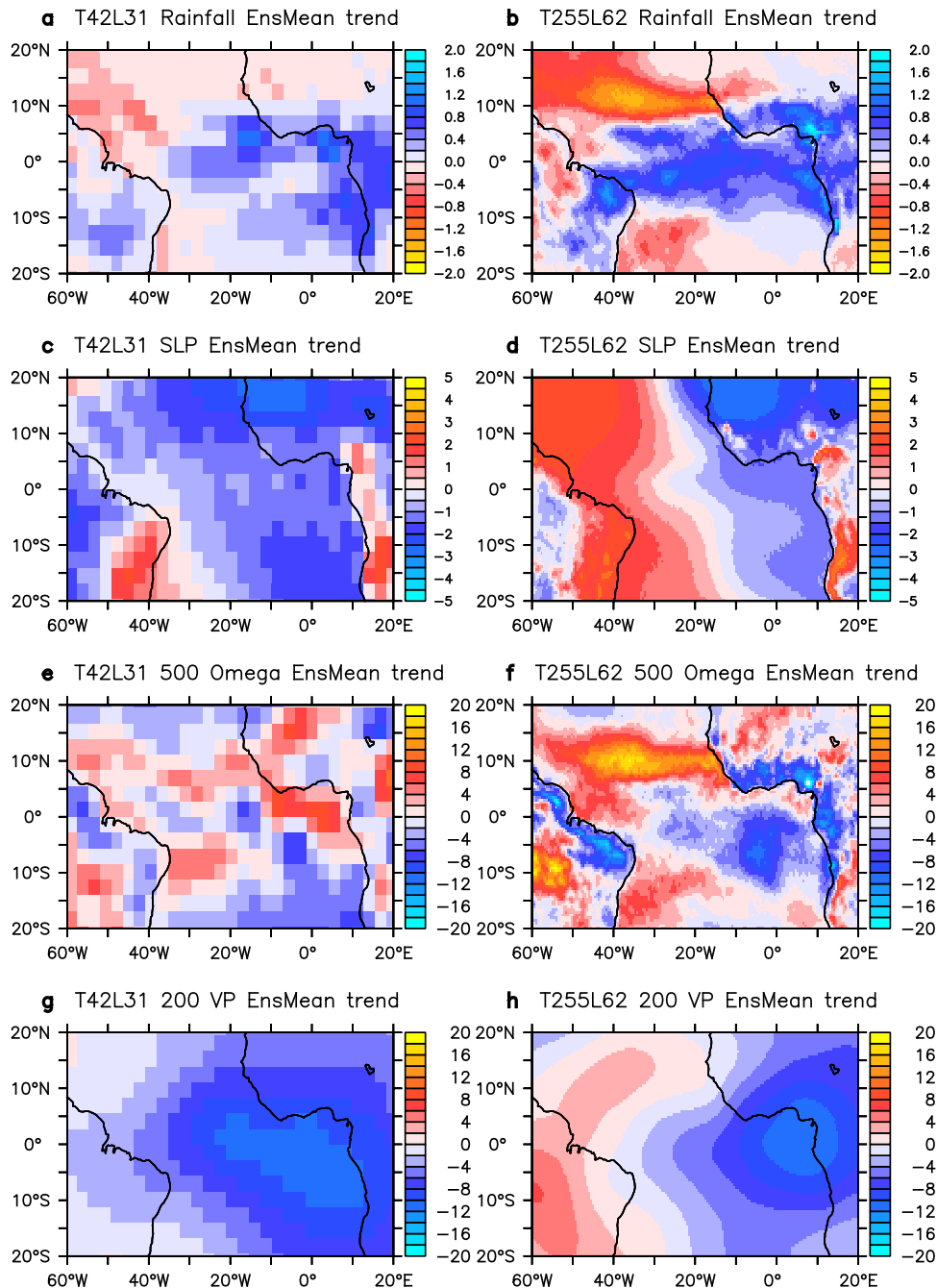


Fig. 3 Atmospheric changes. Ensemble-mean trends, calculated over all 70 years, of **a, b** rainfall (mm day⁻¹ per 70 years), **c, d** normalized sea level pressure (SLP), **e, f** vertical velocity at 500 hPa (10⁻³ Pa s⁻¹ per 70 years) negative upward), and **g, h** velocity potential at 200 hPa (10⁵ m² s⁻² per 70 years) calculated from KCM-LR (**a, c, e, g**) and from KCM-HR (**b, d, f, h**). Note that SLP is normalized by its standard deviation at each grid points prior to the trend analysis.

KCM-HR (Fig. 3b) is reproduced (Fig. 5a). However, the marked drying north of the equatorial region is not simulated in experiment TA. If the SST trends only are specified over the tropical Indo-Pacific (Fig. 5b) or globally outside of the TA (Fig. 5c), the rainfall is reduced over the equatorial Atlantic. The experiments with ECHAM5-HR thus suggest that it is mainly the local TA-SST changes that force the increased rainfall over the equatorial Atlantic in KCM-HR. On the other hand, some of the drying observed in KCM-HR over the off-equatorial regions is reproduced in experiments TIP and nTA. Thus, remote forcing appears to be important in the off-equatorial regions. It is noteworthy that in none of the AGCM experiments the rainfall trend pattern

simulated by KCM-HR is fully captured (Fig. 3b). This may be due to the lack of atmosphere–ocean coupling or to nonlinearities, because SST trends only were specified in selected regions.

We next investigate AGCM's rainfall sensitivity to (1) SST-trend pattern, (2) mean state, and (3) model resolution.

- (1) The sensitivity to the SST-trend pattern is assessed by comparing the above AGCM-results (Figs. 5a and 6b) with an experiment in which the SST trends from KCM-LR (Fig. 1e and Supplementary Fig. 2b) are prescribed over the TA (Fig. 6a). ECHAM5-HR's rainfall sensitivity to the SST-trend pattern is shown by the differences in response (Fig. 6c). The

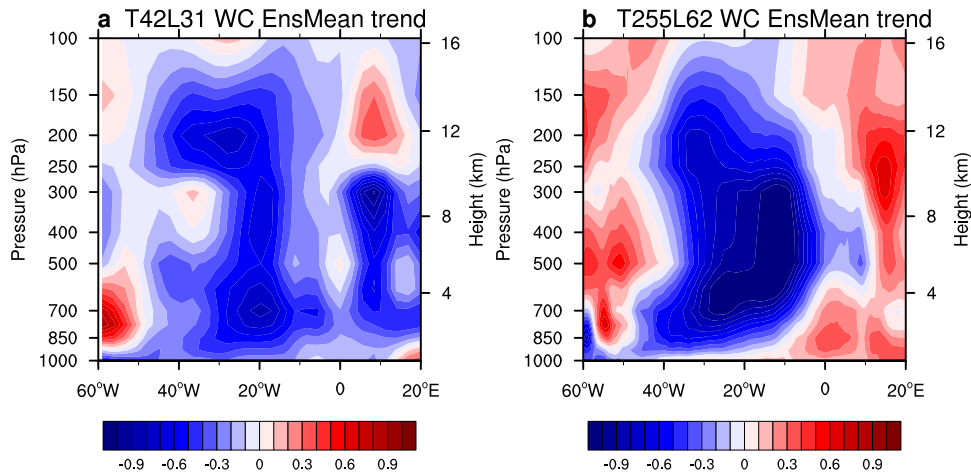


Fig. 4 Walker circulation change. Changes in the Walker circulation at the equator (5°N – 5°S), as expressed by the zonal mass streamfunction ($10^{10} \text{ kg s}^{-1}$ per 70 years). Shown are ensemble-mean trends, calculated over all 70 years, from **a** KCM-LR and **b** from KCM-HR.

Table 1. Summary of the AGCM simulations forced by prescribed SSTs.

Forcing region	SST trend taken from	Observed SST	KCM-HR SST climatology	KCM-LR SST climatology
(Control)		Clim _{Obs}	Clim _{T255L62}	Clim _{T42L31}
Tropical Atlantic	KCM-HR	TA _{SST} T255L62	TA _{SST} T255L62	TA _{SST} T255L62
	KCM-LR	TA _{SST} T42L31	TA _{SST} T42L31	TA _{SST} T42L31
Tropical Indo-Pacific	KCM-HR	TIP _{SST} T255L62		
	KCM-LR	TIP _{SST} T42L31		
Global, outside Tropical Atlantic	KCM-HR	nTA _{SST} T255L62		
	KCM-LR	nTA _{SST} T42L31		

dependence of the trend-pattern sensitivity on the background mean-state SST, on which the SST trends are superimposed, is assessed by additional simulations in which the TA-SST trends are superimposed on the SST climatologies calculated from KCM-LR and KCM-HR. Again, simulations with the respective climatological SSTs are conducted to determine the rainfall responses (Fig. 6d, e, g, h). This yields two additional estimates of the rainfall sensitivity to the SST-trend pattern. All three estimates (Fig. 6c, f, i) are similar, indicating that the TA-SST trends in KCM-HR, in comparison to that in KCM-LR, favor enhanced rainfall over the eastern half of the equatorial TA and reduced rainfall over the northern and southern TA. We note that the sensitivity is larger when a model climatology is used (Fig. 6f, i) instead of the observed climatology (Fig. 6c), especially when the climatology of KCM-HR is used (Fig. 6f).

- (2) We assess the influence of the mean-state SST on the rainfall response. To this end we compare experiments forced by an identical SST-trend pattern (obtained from either KCM-LR or KCM-HR) that is superimposed on the SST climatologies derived from KCM-HR (Fig. 6d, e) and KCM-LR (Fig. 6g, h). The mean-state SST sensitivity of the rainfall response is quite large and does not strongly depend on the choice of the SST-trend pattern (Fig. 6j, k). This suggests that the SST bias plays an important role in shaping the rainfall response to increasing CO_2 levels. In comparison to KCM-LR's mean-state

SST, that of KCM-HR favors increased rainfall over the equatorial belt and over western Africa in the region 10°N – 10°S (Fig. 6k). Much-reduced rainfall is favored over the southeastern TA when using KCM-HR's mean-state SST, the region where the warm bias in KCM-LR is largest (Fig. 1d), and north of the equator.

- (3) Finally, the sensitivity of the rainfall response to model resolution is investigated. This sensitivity is assessed by repeating the experiments conducted with ECHAM5-HR (T255L62) with ECHAM5-LR (T42L31). The former are shown in Fig. 6a–k, the latter in Supplementary Fig. 3a–k. Overall the simulations with ECHAM5-HR and ECHAM5-LR yield similar patterns and the derived sensitivities are similar too. There are, however, noticeable differences. For example, when the TA-SST trends from KCM-HR are applied, in comparison with ECHAM5-LR, ECHAM5-HR simulates stronger rainfall over the eastern TA and weaker rainfall over the western TA (Fig. 6l), where Fig. 6l is the difference between the two responses, i.e., the difference between Fig. 6e and Supplementary Fig. 3e.

It can be concluded from the set of uncoupled atmosphere model experiments that all three factors, SST-trend pattern, mean-state SST, and atmosphere model resolution contribute to the differences in equatorial rainfall response between KCM-HR and KCM-LR (Supplementary Fig. 3l). The mean-state SST, however, yields the overall largest contributions to the differences. All three factors support enhanced rainfall over the eastern equatorial Atlantic, especially the SST-trend pattern, which is an expression of the deep atmospheric response in KCM-HR. The largest contribution outside the equatorial region stems from the mean-state SST, particularly over the southeastern TA, suggesting that the strength of the warm bias there plays the most important role. Remote forcing plays a role off the equator. Finally, we note that uncoupled experiments only can be an approximation to what is simulated in fully coupled mode.

DISCUSSION

This study suggests that the projected TA-sector climate response to rising atmospheric CO_2 -concentrations could be sensitive to atmospheric resolution, which influences the strength of the warm bias over the eastern TA. A climate model employing a low-resolution atmosphere and exhibiting a large warm bias, as that observed in many climate models, simulates a zonally uniform equatorial SST response, whereas a model of the same family employing a high-resolution atmosphere and exhibiting a small

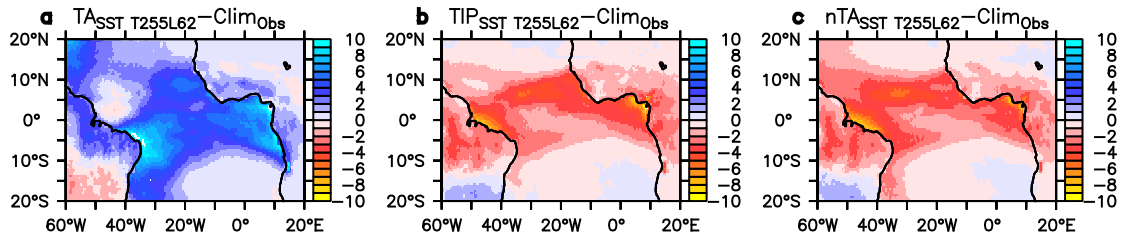


Fig. 5 Role of local and remote SST forcing. **a–c** Rainfall response (mm day^{-1}) of the AGCM ECHAM5 with T255L62 resolution (ECHAM5-HR) forced by the SST trends taken from KCM-HR (see Fig. 1h). Observed monthly-mean SST climatology is used. **a** Rainfall response when the SST trends only are applied over the Tropical Atlantic (TA, 20°S – 20°N), **b** the Tropical Indo-Pacific domain (TIP, 20°S – 20°N) and **c** outside of the Tropical Atlantic (nTA).

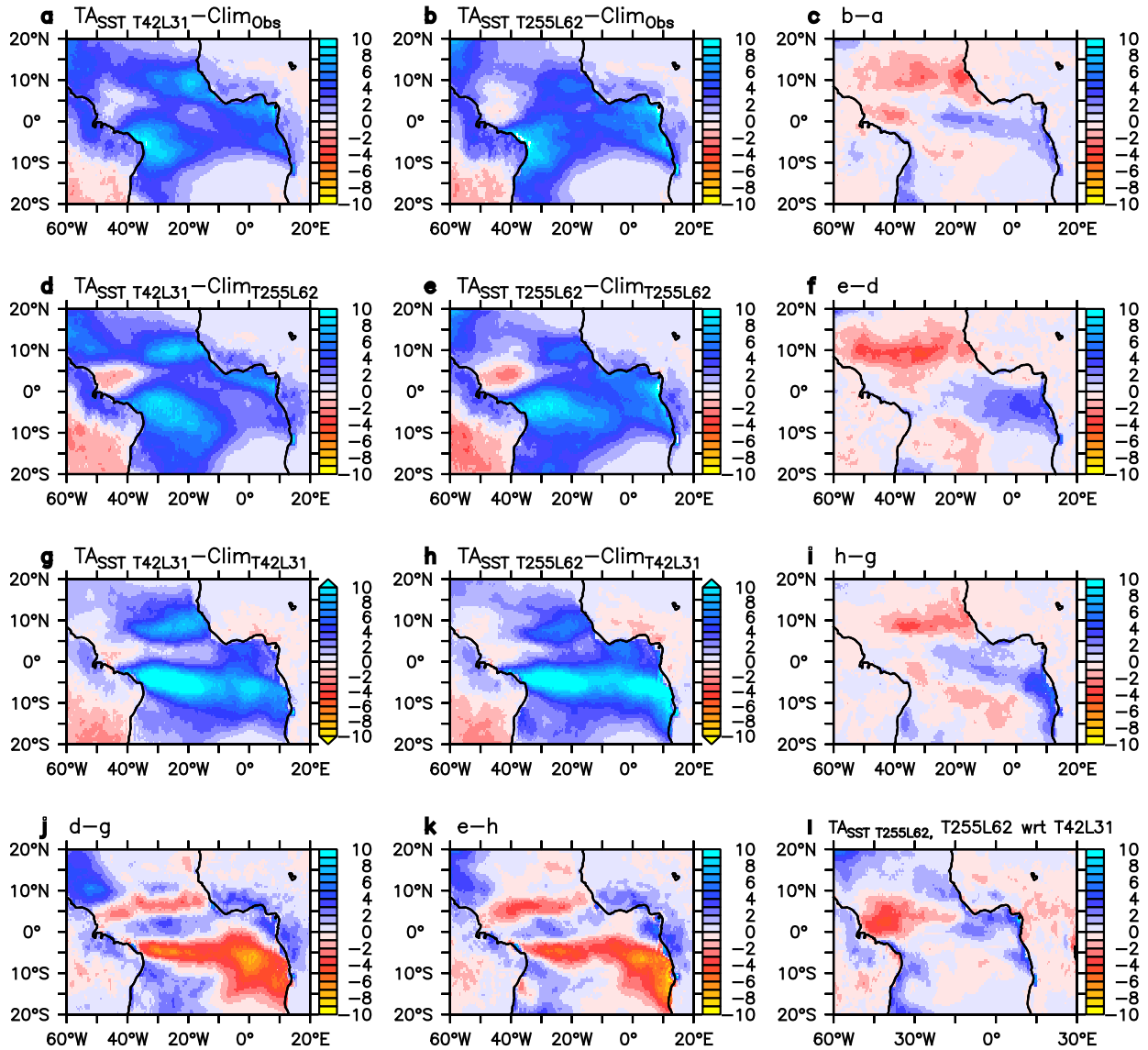


Fig. 6 Rainfall response in high-resolution AGCM. Rainfall response (mm day^{-1}) of the AGCM ECHAM5 with T255L62 resolution (ECHAM5-HR) forced by the SST trends taken from KCM-LR (**a**; see Fig. 1e) and KCM-HR (**b**; see Fig. 1h). **c** The difference between the rainfall responses obtained when forcing ECHAM5-HR by the SST trends over the TA simulated by either KCM-HR or KCM-LR, i.e., **b** minus **a**. Observed monthly-mean SST climatology is used. Same as in **a–c** except that monthly-mean SST climatology is taken from KCM-HR (**d–f**) or KCM-LR (**g–i**). The difference between the rainfall responses to the SST trends from KCM-LR (**j**) and KCM-HR (**k**) over the TA either superimposed on the background SST climatology from KCM-HR or KCM-LR. **l** The difference between the rainfall responses to the SST trends from KCM-HR over the TA either simulated by ECHAM5-HR or ECHAM5-LR, providing information about response sensitivity to atmospheric resolution. **c, f, i** Impact of the SST-trend pattern: difference between the rainfall responses obtained when forcing ECHAM5-HR by the SST trends over the TA simulated by either KCM-HR or KCM-LR. **j, k** Mean-state impact: difference between the rainfall responses to the SST trends from KCM-HR over the TA, superimposed either on the monthly SST climatology from KCM-LR (**j**) or KCM-HR (**k**).

warm bias simulates a pronounced eastward amplification of the SST warming that can be roughly characterized as Atlantic Niño- or zonal mode-like. Further, in both climate models the SST response to increasing atmospheric CO₂-levels bears resemblance to the pattern of internal SST variability with respect to its maximum. Finally, the model exhibiting a large warm bias and zonally uniform equatorial SST response only simulates strong atmospheric changes over limited regions of the TA, while the model exhibiting a relatively small warm bias and an eastward amplified equatorial SST response simulates much stronger and basin-wide changes in atmospheric circulation. We argue that the markedly different atmospheric response is mostly due to the differences in the equatorial SST response which is sensitive to atmospheric resolution that also impacts warm bias strength.

One may anticipate that a less-biased model yields more reliable climate projections for the future. This conjecture is supported by the observed SST trends since the mid-20th century, which are characterized by a basin-wide SST warming with a maximum over the southeastern TA, a pattern that shares similarities with the CO₂-induced warming trends simulated by KCM-HR. Further, the observed SST-trend pattern bears resemblance to the pattern of interannual SST variability. In particular, the SST warming is large in the cold-tongue region of the eastern TA where interannual variability is large too. This also is consistent with the results from KCM-HR. However, we do not know whether the observed warming trends over the TA are forced by rising atmospheric CO₂-concentrations or due to long-term natural variability. If the observed trends are CO₂-forced, alleviating the warm bias could constitute a major step forward to improve climate change projections over the TA sector. The downscaling of the climate response to anthropogenic forcing obtained from global climate models to regional or local scale is an important step to inform decision makers. However, climate model bias is still an issue and previous studies have questioned the application of conventional bias-correction methods in the presence of overly large biases³⁰. Our model results suggest that the warm bias over the TA appears to be greatly reducible by enhancing the atmospheric resolution in climate models, which may enable more meaningful downscaling approaches. Results from other climate models in support of the KCM's results will be discussed in a forthcoming paper.

METHODS

Coupled general circulation model

We employ two versions of the KCM. Its ocean component is NEMO³¹ with a horizontal resolution of 2° (ORCA2 grid) including a latitudinal refinement of 0.5° close to the equator and 31 vertical levels. The atmospheric component is the AGCM ECHAM5³². Two configurations of the KCM are used here, which only differ in atmosphere model resolution²⁴: one carries ECHAM5 with a horizontal resolution of T42 (~2.8°) and 31 vertical levels (labeled KCM-LR), and the other ECHAM5 with a horizontal resolution of T255 (~0.47°) and 62 levels (labeled KCM-HR). The additional vertical levels in KCM-HR are placed in between the 31 vertical levels used in KCM-LR and concentrate toward the surface. The top atmospheric level is the same in both configurations and at 10 hPa. No re-tuning of the KCM was performed when changing the atmosphere model resolution.

We have performed two types of simulations with each KCM version: first, a control run with constant present-day atmospheric CO₂-concentration amounting to 348 ppm. Second, initialized with data from the control run, a climate change ensemble in which the atmospheric CO₂-concentration increases at a rate of 1% per year until it doubles at 696 ppm after 70 years. Each ensemble consists of five members starting from different ocean and atmospheric conditions taken every 10 years from the control run. Although the two versions of the KCM exhibit rather different SST biases over the TA, the transient climate sensitivity is quite similar, as shown by the ensemble-mean GSAT (Supplementary Fig. 1): at the time of CO₂-doubling, the GSAT increases by 2.2 °C in both models. Annual-mean data are used for the analysis and ensemble means are shown.

Atmosphere general circulation model (AGCM)

We additionally conducted stand-alone integrations with the high-resolution (T255L62) and coarse-resolution (T42L31) AGCM ECHAM5 forced by prescribed monthly SST, termed ECHAM5-HR and ECHAM5-LR, respectively. Four integrations for each resolution are performed: first, a control run forced by observed monthly SST climatology (AMIP SST). Second, the SST trends from KCM-HR (Fig. 1h) are added to the SST climatology for each month over the TA (20°S–20°N). Third, the SST trends from KCM-HR are added over the tropical Indo-Pacific basin (20°S–20°N). Third, the SST trends from KCM-HR are added outside of the TA. Fourth, the SST trends from KCM-LR (Fig. 1e) are added to the SST climatology over the TA (20°S–20°N). Note that the SST trends are calculated from the annual-mean data, and these trends are added in all calendar months. Integration length amounts to 9 (29) years for ECHAM5-HR (LR), and averages computed over the whole integration time are used in the analyses. It is noteworthy that the average rainfall from ECHAM5-LR calculated from the first 9 and all 29 years does not significantly differ.

In addition to using observed monthly SST climatology when adding SST trends from KCM-HR or KCM-LR over the TA, we use monthly SST climatology from the control simulations with KCM-LR and KCM-HR. This enables investigating the atmospheric response sensitivity to varying mean state caused by varying SST climatology. The AGCM simulations conducted for this study are summarized in Table 1. Only rainfall is shown from the uncoupled integrations with ECHAM5-LR and ECHAM5-HR.

DATE AVAILABILITY

The datasets generated during and/or analyzed during the current study are available from the corresponding author on reasonable request.

Received: 13 November 2019; Accepted: 27 August 2020;

Published online: 15 September 2020

REFERENCES

- Pachauri, R. K. et al. Climate Change 2014: *Synthesis Report. Contribution of Working Groups I, II and III to the Fifth Assessment Report of the Intergovernmental Panel on Climate Change* (IPCC, 2014).
- van Vuuren, D. P. et al. The representative concentration pathways: an overview. *Clim. Chang.* **109**, 5–31 (2011).
- Stouffer, R. J. & Manabe, S. Assessing temperature pattern projections made in 1989. *Nat. Clim. Chang.* **7**, 163–165 (2017).
- Wang, C. Z., Zhang, L. P., Lee, S. K., Wu, L. X. & Mechoso, C. R. A global perspective on CMIP5 climate model biases. *Nat. Clim. Chang.* **4**, 201–205 (2014).
- Deser, C., Phillips, A. S., Alexander, M. A. & Smoliak, B. V. Projecting North American climate over the next 50 years: uncertainty due to internal variability. *J. Clim.* **27**, 2271–2296 (2014).
- Biasutti, M., Held, I. M., Sobel, A. H. & Giannini, A. SST forcings and Sahel rainfall variability in simulations of the twentieth and twenty-first centuries. *J. Clim.* **21**, 3471–3486 (2008).
- Cook, K. H. Climate science: the mysteries of Sahel droughts. *Nat. Geosci.* **1**, 647–648 (2008).
- Hawkins, E. & Sutton, R. The potential to narrow uncertainty in regional climate predictions. *Bull. Am. Meteor. Soc.* **90**, 1095–1108 (2009).
- Park, J. Y., Bader, J. & Matei, D. Northern-hemispheric differential warming is the key to understanding the discrepancies in the projected Sahel rainfall. *Nat. Commun.* **6**, 5985 (2015).
- Tebaldi, C., Arblaster, J. M. & Knutti, R. Mapping model agreement on future climate projections. *Geophys. Res. Lett.* **38**, L23701 (2011).
- Exarchou, E., Prodhomme, C., Brodeau, L., Guemas, V. & Doblas-Reyes, F. Origin of the warm eastern tropical Atlantic SST bias in a climate model. *Clim. Dyn.* **51**, 1819–1840 (2018).
- Grodsky, S. A., Carton, J. A., Nigam, S. & Okumura, Y. M. Tropical Atlantic biases in CCSM4. *J. Clim.* **25**, 3684–3701 (2012).
- Li, G. & Xie, S. P. Origins of tropical-wide SST biases in CMIP multi-model ensembles. *Geophys. Res. Lett.* **39**, L22703 (2012).
- Richter, I., Xie, S. P., Behera, S. K., Doi, T. & Masumoto, Y. Equatorial Atlantic variability and its relation to mean state biases in CMIP5. *Clim. Dyn.* **42**, 171–188 (2014).
- Richter, I., Xie, S. P., Wittenberg, A. T. & Masumoto, Y. Tropical Atlantic biases and their relation to surface wind stress and terrestrial precipitation. *Clim. Dyn.* **38**, 985–1001 (2012).
- Volodro, A. et al. Role of wind stress in driving SST biases in the Tropical Atlantic. *Clim. Dyn.* **53**, 3481–3504 (2019).

17. Wahl, S., Latif, M., Park, W. & Keenlyside, N. On the tropical Atlantic SST warm bias in the Kiel Climate Model. *Clim. Dyn.* **36**, 891–906 (2009).
18. Richter, I. & Xie, S. P. On the origin of equatorial Atlantic biases in coupled general circulation models. *Clim. Dyn.* **31**, 587–598 (2008).
19. Xu, Z., Chang, P., Richter, I., Kim, W. & Tang, G. L. Diagnosing southeast tropical Atlantic SST and ocean circulation biases in the CMIP5 ensemble. *Clim. Dyn.* **43**, 3123–3145 (2014).
20. Ding, H., Keenlyside, N., Latif, M., Park, W. & Wahl, S. The impact of mean state errors on equatorial Atlantic interannual variability in a climate model. *J. Geophys. Res. Oce.* **120**, 1133–1151 (2015).
21. Hsu, W.-C., Patricola, C. M. & Chang, P. The impact of climate model sea surface temperature biases on tropical cyclone simulations. *Clim. Dyn.* **53**, 173–192 (2018).
22. Park, W. et al. Tropical Pacific Climate and its response to global warming in the Kiel Climate Model. *J. Clim.* **22**, 71–92 (2009).
23. Harlaß, J., Latif, M. & Park, W. Improving climate model simulation of tropical Atlantic sea surface temperature: The importance of enhanced vertical atmosphere model resolution. *Geophys. Res. Lett.* **42**, 2401–2408 (2015).
24. Harlaß, J., Latif, M. & Park, W. Alleviating tropical Atlantic sector biases in the Kiel climate model by enhancing horizontal and vertical atmosphere model resolution: climatology and interannual variability. *Clim. Dyn.* **50**, 2605–2635 (2017).
25. Steinig, S., Harlass, J., Park, W. & Latif, M. Sahel rainfall strength and onset improvements due to more realistic Atlantic cold tongue development in a climate model. *Sci. Rep.* **8**, 2569 (2018).
26. Milinski, S., Bader, J., Haak, H., Siongo, A. C. & Jungclaus, J. H. High atmospheric horizontal resolution eliminates the wind-driven coastal warm bias in the southeastern tropical Atlantic. *Geophys. Res. Lett.* **43**, 10455–10462 (2016).
27. Taylor, K. E., Stouffer, R. J. & Meehl, G. A. An overview of CMIP5 and the experiment design. *Bull. Am. Meteor. Soc.* **93**, 485–498 (2012).
28. Lübbecke, J. F. et al. Equatorial Atlantic variability—modes, mechanisms, and global teleconnections. *Wiley Interdiscip. Rev. Clim. Chang.* **9**, e527 (2018).
29. Enfield, D. B. & Mayer, D. A. Tropical Atlantic sea surface temperature variability and its relation to El Niño Southern Oscillation. *J. Geophys. Res. Oceans.* **102**, 929–945 (1997).
30. Maraun, D. et al. Towards process-informed bias correction of climate change simulations. *Nat. Clim. Chang.* **7**, 764–773 (2017).
31. Madec, G. NEMO ocean engine. Note du Pole de modélisation 27, Institut Pierre-Simon Laplace (2008).
32. Roeckner, E. et al. Sensitivity of simulated climate to horizontal and vertical resolution in the ECHAM5 atmosphere model. *J. Clim.* **19**, 3771–3791 (2006).
33. Huang, B. et al. Extended reconstructed sea surface temperature, Version 5 (ERSSTv5): Upgrades, validations, and intercomparisons. *J. Clim.* **30**, 8179–8205 (2017).

ACKNOWLEDGEMENTS

This study was supported by the InterDec project “The potential of seasonal-to-decadal-scale inter-regional linkages to advance climate predictions” of the JPI CLIM

Belmont-Forum, and by the RACE “Regional Atlantic Circulation and Global Change” Project of the BMBF. We thank Dr. Jan Harlaß for providing a configuration of the T255L62 version of the KCM. The climate model integrations were performed at the Computer Centre at the Kiel University and at the High Performance Computing Centre (HRLN). Open access funding provided by Projekt DEAL.

AUTHOR CONTRIBUTIONS

M.L. suggested the study. M.L. and W.P. jointly interpreted the results and M.L. wrote the first draft. W.P. conducted simulations and analyses. Correspondence and requests for materials should be addressed to wpark@geomar.de.

COMPETING INTERESTS

The authors declare no competing interests.

ADDITIONAL INFORMATION

Supplementary information is available for this paper at <https://doi.org/10.1038/s41612-020-00139-6>.

Correspondence and requests for materials should be addressed to W.P.

Reprints and permission information is available at <http://www.nature.com/reprints>

Publisher’s note Springer Nature remains neutral with regard to jurisdictional claims in published maps and institutional affiliations.



Open Access This article is licensed under a Creative Commons Attribution 4.0 International License, which permits use, sharing, adaptation, distribution and reproduction in any medium or format, as long as you give appropriate credit to the original author(s) and the source, provide a link to the Creative Commons license, and indicate if changes were made. The images or other third party material in this article are included in the article’s Creative Commons license, unless indicated otherwise in a credit line to the material. If material is not included in the article’s Creative Commons license and your intended use is not permitted by statutory regulation or exceeds the permitted use, you will need to obtain permission directly from the copyright holder. To view a copy of this license, visit <http://creativecommons.org/licenses/by/4.0/>.

© The Author(s) 2020